Article

Rapid Electrochemical Methane Functionalization Involves Pd–Pd Bonded Intermediates

R. Soyoung Kim, Evan C. Wegener, Min Chieh Yang, Matthew E. O'Reilly, Seokjoon Oh, Christopher H. Hendon,* Jeffrey T. Miller,* and Yogesh Surendranath*

Read Online

ACCESS | 📊 Metrics & More | 📰 Article Recommendations | 🆂🅸 Supporting Information

ABSTRACT: High-valent Pd complexes are potent agents for the oxidative functionalization of inert C–H bonds, and it was previously shown that rapid electrocatalytic methane monofunctionalization could be achieved by electro-oxidation of Pd^{II} to a critical dinuclear Pd^{III} intermediate in concentrated or fuming sulfuric acid. However, the structure of this highly reactive, unisolable intermediate, as well as the structural basis for its mechanism of electrochemical formation, remained elusive. Herein, we use X-ray absorption and Raman spectroscopies to assemble a structural model of the potent methane-activating intermediate as a Pd^{III} dimer with a Pd–Pd bond and a 5-fold O atom coordination by $H_xSO_4^{(x-2)}$ ligands at each Pd center. We further use EPR spectroscopy to identify a mixed-valent M–M bonded $Pd_2^{II,III}$ species as a key intermediate during the Pd^{II}-to-Pd^{III}_2 oxidation. Combining EPR and electrochemical data, we quantify the free energy of Pd dimerization as <-4.5 kcal/mol for $Pd_2^{II,III}$ and <-9.1 kcal/mol for Pd^{III}_2. The structural and thermochemical data suggest that the aggregate effect of metal–metal and axial metal–ligand bond formation drives the critical Pd dimerization reaction in between electrochemical oxidation steps. This work establishes a structural basis for the facile electrochemical oxidation of Pd^{II} to a M–M bonded Pd^{III} dimer and provides a foundation for understanding its rapid methane functionalization reactivity.
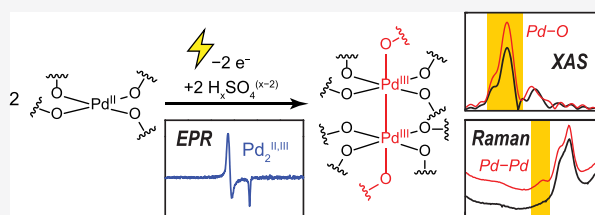
INTRODUCTION

Metal–metal bonded species are increasingly recognized as key catalytic intermediates.[1−3] Metal–metal bonding plays a particularly important role in high-valent Pd catalysis. While catalysis by Pd was initially understood as mononuclear $Pd^{0/II}$ cycles, along with Pd^{IV} intermediates, metal–metal bonded Pd^{III} dimers have been isolated and proposed to play a key role in C–X and C–C bond formations.[4−8] Bimetallic cooperativity was suggested to lower the barriers for oxidation of organometallic Pd^{II} precursors and accelerate the subsequent reductive elimination from Pd^{III} dimers.[9,10] Furthermore, Pd^{III} intermediates of various structures have also been invoked in other types of reactions such as aerobic hydroxylation, radical C–C coupling, and halogen addition to alkenes.[7,11] However, the structures of high-valent Pd intermediates in catalytic transformations often remain elusive because of their high reactivity and propensity to undergo rapid reductive elimination. Furthermore, the structure of high-valent Pd intermediates and their mechanism of formation are strongly dependent on many factors, including the supporting ligands, type of oxidant, and solvent.[12−18] Thus, expanding the palette of structurally characterized high-valent Pd catalytic intermediates and elucidating the structural factors that contribute to their formation would enable more systematic access to their rich oxidation reactivity.

Electrochemistry offers high and tunable driving forces for accessing reactive intermediates at low temperatures while avoiding the use of expensive stoichiometric reagents.[19,20] Leveraging this quality, we showed that $Pd^{II}SO_4$ in concentrated or fuming sulfuric acid could be electrochemically oxidized to a novel high-valent Pd intermediate.[21] This species then monofunctionalized the inert C–H bonds of methane with rates ~20-fold faster than state-of-the-art Pt^{II}-based homogeneous catalysts[22] and ~5000-fold faster than Pd^{II} under similar conditions.[21] This rare example of C–H activation at a high-valent Pd species, combined with the exceptional reaction rates, motivated detailed inquiry into the identity of the operative high-valent species and its mechanism of formation. On the basis of cyclic voltammetry and methane reaction stoichiometry, we proposed the formation of a dinuclear Pd^{III}_2 complex upon electrochemical oxidation of Pd^{II}. Specifically, we proposed an *ECE* mechanism, in which a chemical step (*C*) occurs between two distinct electron transfer steps (*E*), with the second electron transfer being
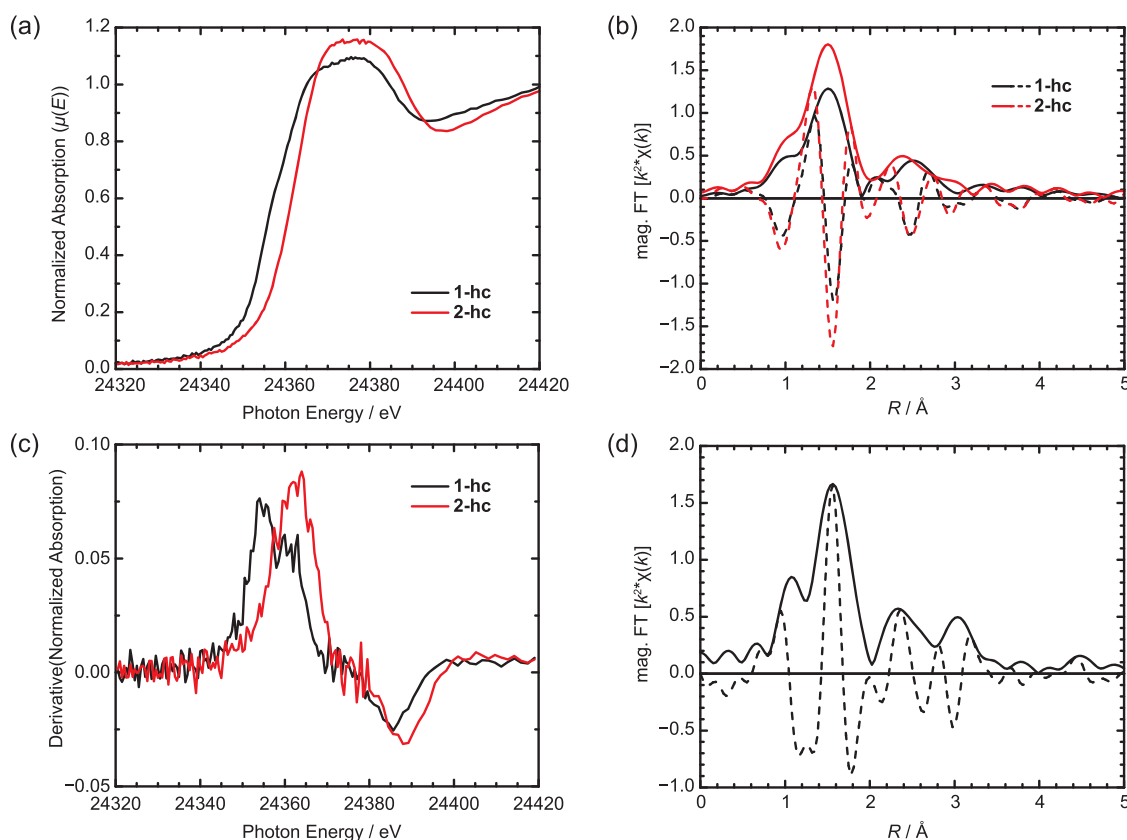
Figure 1. Pd K-edge X-ray absorption spectra of **1-hc** and **2-hc**: (a) XANES; (b) EXAFS showing the real (solid line) and imaginary (dashed line) components; (c) first derivative of the XANES, where the **lc** samples showed essentially identical results (Figures S6−S9); (d) Pt K-edge EXAFS of Pt^{III}_2 in the solid state.

thermodynamically favored relative to the first. Through this unusual *ECE* mechanism, this Pd electrocatalyst is able to aggregate 1-e⁻-at-a-time electrochemical oxidation events to generate a potent 2-e⁻ Pd^{III}_2 oxidant for rapid methane functionalization.

These studies, however, provided negligible insight into the structure of the critical Pd^{III}_2 species or the intermediates along its formation mechanism. In particular, the nature of the metal−metal interaction in Pd^{III}_2 remains unknown. Whereas many Pd^{III}_2 complexes[23,24] contain direct Pd−Pd bonds, the Pd centers can also be linked through one or more bridging ligands.[25,26] Furthermore, most metal−metal bonded Pd^{III}_2 complexes are obtained via oxidation of cofacially oriented, ligand-bridged, dinuclear Pd^{II}_2 complexes in which the Pd centers are predisposed toward facile M−M bond formation using two-electron chemical oxidants. In contrast, our Pd^{III}_2 complex is generated via sequential one-electron electrochemical oxidation from a simple mononuclear Pd^{II}(sulfate) complex, leaving open the critical questions of whether a M−M bond exists in the Pd^{III}_2 species and what role it plays in fostering the unusual *ECE* electrochemical oxidation mechanism. Given the key role of M−M bonding in high-valent Pd oxidation catalysis,[2] addressing these structural and mechanistic knowledge gaps is critical for the rational design of oxidative electrocatalysis with high-valent Pd intermediates.[27]

Herein, we establish the core structure of the electrochemically generated Pd^{III}_2 and provide a structural basis for its unique mechanism of formation. Since the Pd^{III}_2 complex cannot be isolated from the sulfuric acid medium, we combine X-ray absorption and Raman spectroscopies to establish that it

contains a Pd−Pd bond with each Pd atom coordinated by five O atoms. Against this backdrop, we use EPR spectroscopy to identify a mixed-valent intermediate in the *ECE* reaction sequence and combine these data with electrochemical measurements to map the thermodynamic landscape that drives the dimerization of the two Pd centers. Analysis of our results and previous electrochemical studies in the literature reveals the importance of the Pd−Pd bond and axial ligand coordination for enabling the electrochemical oxidation and dimerization of Pd^{II} to Pd^{III}_2. These insights provide a foundation for understanding the unusual reactivity of Pd^{III}_2 and for electrochemically generating new high-valent Pd complexes that may enable challenging oxidation reactions.

■ RESULTS AND DISCUSSION

Structure of Pd^{III}_2. *Sample Preparation.* The Pd^{III}_2 sample for spectroscopic investigation was generated by bulk electrolysis of $Pd^{II}SO_4$, in fuming H_2SO_4 containing 18−24% SO_3 by weight. We designate the pre- and postelectrolysis samples as **1** and **2**, respectively. **2** displays a strong absorbance at 300 nm,[21] which allowed us to monitor the progress of the electrolysis by UV−vis spectroscopy. The anhydrous medium is critical to the stability of the high-valent species, which undergoes spontaneous reduction in nonfuming H_2SO_4 presumably via solvent oxidation ($H_2SO_4 \rightarrow {}^1/_2O_2 + SO_3 + 2e^- + 2H^+$). The solubility of $Pd^{II}SO_4$ was limited to ~10 mM; in our effort to increase the signal-to-noise ratio of our measurements, we found that addition of 1.4 M $(NH_4)_2SO_4$ increased Pd^{II} solubility to ~50 mM.[28] Voltammetric, spectroscopic, and methane reactivity studies all indicated

that electrolysis in the presence of $(NH_4)_2SO_4$ generates the same Pd^{III}_2 complex (Figures S2, S4, S6−S9 and Table S1). Thus, low and high concentration samples of **1** and **2**, designated as **1/2-lc** and **1/2-hc**, were prepared in the absence and presence of $(NH_4)_2SO_4$, respectively, for further analysis.

X-ray Absorption Spectroscopy. X-ray absorption near edge structure (XANES) spectra support the formation of a high-valent species upon electro-oxidation of **1** (Figure 1a). Consistent with an increase in oxidation state, the XANES spectrum of **2** displays a rising edge inflection point that is 7.4 eV higher than **1** (Table 1) for both **lc** and **hc** samples.

Table 1. Summary of XAS Results

sample	edge E (keV)	CN_{Pd-O}	R (Å)	σ^2 ($\times 10^3$ Å^2)	E_0 (eV)
1, solid	24.3550	4.0	2.01	1.4	1.2
1-lc	24.3550	4.0	2.00	3.0	−0.3
1-hc	24.3550	4.0	2.01	1.2	−0.2
2-lc	24.3624	5.0	2.00	2.7	2.6
2-hc	24.3624	5.2	1.98	0.9	2.8
Pt^{III}_2, solid	11.5660	5.0	1.98	3.2	−2.2

Repeated measurements on the same sample did not show any shift in the edge energy, indicating that the complex was not subject to X-ray photodegradation over the time scale of the measurement. Importantly, the XANES spectrum of **2** displays a smooth rising edge. This implies a uniform Pd oxidation state and argues against the presence of a mixed-valent dinuclear species such as $Pd^{II}-Pd^{IV}$, which has been demonstrated in the presence of disparate apical ligand environments.[2,18]

Extended X-ray absorption fine structure (EXAFS) spectra indicate that the Pd^{III} centers are each ligated by five oxygen atoms. The Fourier-transformed EXAFS of **1** and **2** in *R*-space both display a prominent peak at 1.5 Å (phase uncorrected distance) arising from the first nearest neighbor scattering interactions (Figure 1b). Since the only ligand present in the system is $H_xSO_4^{(x-2)}$, this peak was isolated and fitted with oxygen scatterers (Table 1). For **1**, the Pd−O coordination number of 4 and average bond distance of 2.01 Å are in line with the known structure of square-planar $Pd^{II}SO_4$.[29] Similar fitting of the Pd^{III}_2 species, **2**, revealed an increase in the number of coordinated O atoms to five and a slight contraction of the average Pd−O bond distance to 1.99 Å. We note that EXAFS provides information about the average local structure, and small differences among Pd−O bond lengths cannot be unambiguously extracted for this system.[30] Known structurally characterized Pd^{III} complexes usually show a distorted pseudo-octahedral coordination,[7] and the change in edge shape, particularly evident in the first derivative of the spectra (Figure 1c), suggests a transition from square-planar to octahedral coordination of the Pd center upon electro-oxidation (see the Supporting Information, section 5 for details).[31−34] Moreover, the diamagnetism of **2**[21] implies electronic coupling between the two d^7 Pd^{III} centers. These observations led us to reason that there should be a Pd as the sixth coordinating atom. Notably, these XAS results rule out the formation of polynuclear 1D chain of Pd^{III} centers.[35]

In principle, the EXAFS of **2** should contain a contribution from Pd−Pd scattering, as has been shown for other M−M bonded compounds.[30,36−39] However, while detection of metal−metal interactions by EXAFS is possible, the assignment depends on the nature of the solvent, the strength of the scattering, and the overlapping scattering from atoms at longer distances.[40,41] Here, we cannot conclusively fit the Pd−Pd scattering peak due to the weak signal beyond the strong first peak and possible interference from multiple scattering paths from sulfurs and oxygens. In an attempt to aid our assignment, we prepared the well-known paddlewheel Pt^{III} dimer with sulfate ligands, $K_2[Pt^{III}_2(SO_4)_4(H_2O)_2]$ (abbreviated as Pt^{III}_2), which features a Pt−Pt bond.[42] The EXAFS of Pt^{III}_2 (Figure 1d) was similar to that of **2** and consistent with five coordinated oxygens (Table 1). The relatively weak features in the higher shell, however, again prevented reliable fitting of the Pt−Pt vector. Since Pd is lighter than Pt, Pd−Pd scattering is weaker than Pt−Pt scattering and more difficult to detect by EXAFS.[43] While this second inconclusive measurement of M−M scattering is not proof of existence of our proposed Pd−Pd interaction, it suggests that EXAFS alone cannot be used to establish the nature of the metal−metal connectivity in this system. Indeed, simulated EXAFS using the computed model structures of Pd^{III}_2 (Figure 4 below) and the known crystal structure of Pt^{III}_2 showed that fitting of the M−M scattering by EXAFS is not feasible due to multiple overlapping scatterings from S and O atoms two or three bonds away (see the Supporting Information, section 9.2 for details).

Raman Spectroscopy. Raman spectra of M−M single bonds are documented for a variety of dinuclear metal complexes[44,45] including Pt^{III}_2.[46] Fortunately, the high mass and relatively weak force constant of M−M single bonds make their vibrations appear in the 100−300 cm^{-1} region, where the spectrum of the fuming H_2SO_4 solvent is relatively featureless (Figure 2a). To confirm our ability to observe the M−M vibration, we acquired the Raman spectra of Pt^{III}_2 (Figure 2b). In fuming H_2SO_4, with or without $(NH_4)_2SO_4$, we observed a peak at 227 cm^{-1} (Figure 2b, orange and red). A similar peak appears at 237 cm^{-1} in 1 M aqueous H_2SO_4 (Figure 2b, blue).
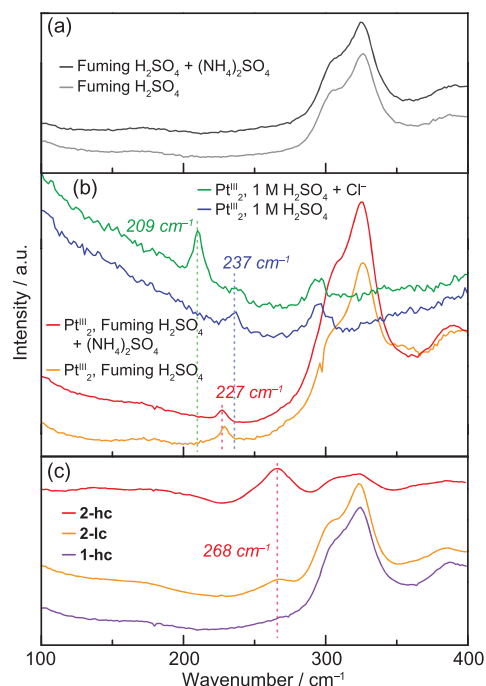

Figure 2. Raman spectra of (a) fuming H_2SO_4; (b) Pt^{III}_2 in fuming H_2SO_4 with or without $(NH_4)_2SO_4$, and in aqueous solutions with or without Cl$^-$; (c) **1** and **2** in fuming H_2SO_4 with or without $(NH_4)_2SO_4$.

Importantly, upon addition of Cl⁻, this peak diminishes and is replaced by a new peak at 209 cm⁻¹ (Figure 2b, green; Figure S10 shows time-dependent evolution of the spectrum). Since Cl⁻ is known to substitute for axial ligands and bind *trans* to the Pt–Pt bond,[46,47] this observation strongly supports the assignment of these peaks to a Pt–Pt vibration.

Encouraged by this result, we collected the Raman spectra of **1** and **2** (Figure 2c). Expectedly, **1** is featureless in the 100–300 cm⁻¹ region (Figure 2c, purple). Contrastingly, both **2-hc** and **2-lc** show a new low energy peak centered at 268 cm⁻¹ (Figure 2c, orange and red), the magnitude of which is much larger in the higher Pd concentration sample. The position of this putative M–M vibrational mode is consistent with the position of the Pt–Pt vibration at 227 cm⁻¹ and the lower atomic mass of Pd.

Moreover, polarized Raman measurements gave identical depolarization ratios for the 227 cm⁻¹ peak of Pt^{III}_2 and the 268 cm⁻¹ peak of **2-hc** (Figure 3) that further support the
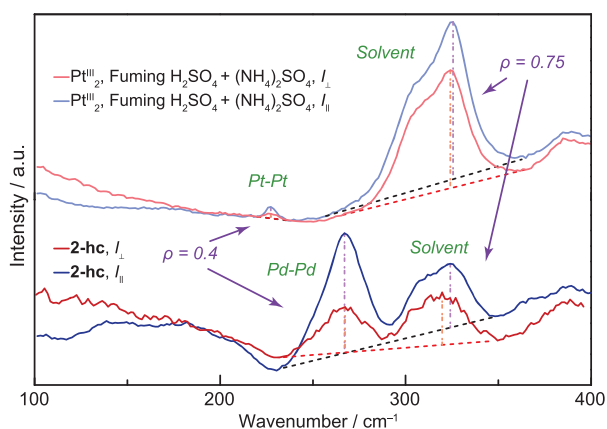

Figure 3. Perpendicular- (red) and parallel- (blue) polarized Raman spectra of Pt^{III}_2 (top) and **2-hc** (bottom). The spectra were scaled to match the depolarization ratio of the solvent peak at 0.75. See the Supporting Information, section 6.2 for details.

assignment of the 227 and 268 cm⁻¹ peaks to M–M stretches in Pt^{III}_2 and Pd^{III}_2, respectively. The depolarization ratio is defined as the ratio of the intensity of scattered light polarized perpendicularly and parallelly to the incident light, and values below 0.75 indicate totally symmetric vibrations. The observed depolarization ratio of ∼0.4 for both the 227 cm⁻¹ peak of Pt^{III}_2 and the 268 cm⁻¹ peak of **2-hc** implies a totally symmetric vibration that is expected for a M–M vibration (see the Supporting Information, section 6.2 for more details).[48,49]

Notably, the 268 cm⁻¹ peak of **2** is much broader than the 227 cm⁻¹ peak of Pt^{III}_2 in the same medium. This may be due to a more labile and dynamic coordination environment of Pd^{III}_2 compared to Pt^{III}_2. Additionally, the spectrum of **2-hc** displays a distorted and attenuated solvent peak at ∼325 cm⁻¹. We speculate that this change in solvent modes may arise from changes in hydrogen bonding caused by the relatively high concentration of Pd^{III}_2 species in the presence of high salt concentration (1.4 M). Together, these analyses lead us to assign the Raman scattering at 268 cm⁻¹ to the vibration of a Pd–Pd bond in Pd^{III}_2.

Structural Model of Pd^{III}_2. In combination, the above studies allow us to assemble a structural model for the Pd^{III}_2 species. X-ray absorption spectroscopy indicates 5-fold coordination by oxygen atoms and an octahedral geometry at

each Pd, and Raman spectroscopy strongly supports the presence of a metal–metal vibrational mode. This allows us to conclude that the structure of our Pd^{III}_2 complex consists of a $(Pd^{III}O_5)_2$ core that is analogous to the known Pt^{III} sulfate dimer. These experimental observations, though, do not yield information about the exact ligand geometry of Pd^{III}_2. Pt^{III}_2 in the solid state is ligated by sulfates in a 4-fold bridging paddlewheel structure with axial aquo ligands, and the relatively narrow Raman band for Pt–Pt vibration is retained across various solvents (Figure 2b), suggesting that this paddlewheel structure persists in solution. In contrast with the relatively narrow Raman peak of Pt^{III}_2, **2** displays an extremely broad Raman signal, suggesting that a simple paddlewheel ligation structure for Pd^{III}_2 is unlikely. Initial computational modeling of Pd^{III}_2 revealed a number of viable conformers and protonation isomers (Figure 4 and Figure
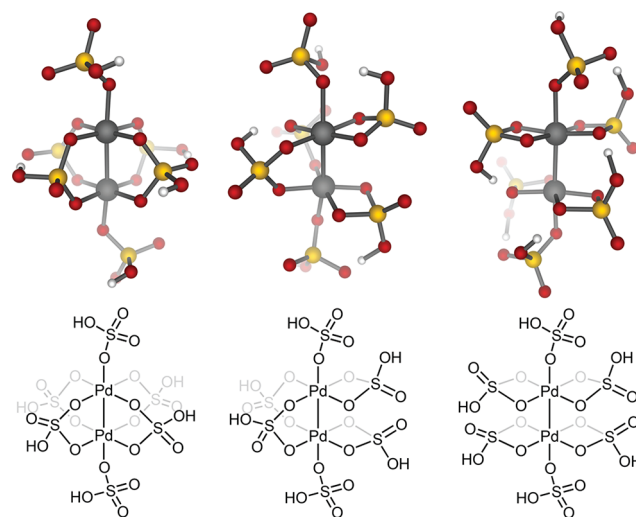

Figure 4. DFT-optimized structures of Pd^{III}_2 with six HSO_4^- ligands with four, two, and zero bridging bisulfates. See the Supporting Information, section 9 for computational details and other isomers that were calculated. White: H. Red: O. Yellow: S. Gray: Pd.

S17), and we are continuing our computational efforts in the context of unraveling the reaction mechanism of methane activation. We note that related ligand binding modes have also been observed for Pd dimers in other oxidation states.[50−53]

Identification and Structural Assignment of a $Pd_2^{II,III}$ Intermediate. *Detection and Assignment of an EPR Signal.* Our previous electrochemical data pointed to an *ECE* mechanism for the formation of Pd^{III}_2 that is detailed below (eqs 1−3; E_1 and E_2 represent standard redox potentials, and $\Delta G_{dim,het}$ stands for the free energy of heterodimerization). This sequence invokes two odd-electron Pd species, Pd^{III} and $Pd_2^{II,III}$, as putative intermediates. We stress that $Pd_2^{II,III}$ is a formal notation that does not imply electron localization. Although our bulk-electrolyzed Pd solution, **2**, is diamagnetic by Evans' method analysis,[21] this solution nonetheless revealed a weak EPR signal at low temperatures that is absent in **1** (Figure 5a). The high anisotropy of this EPR signal indicates that the unpaired electron is metal-based,[54] providing positive evidence for an EPR-active Pd minor component in **2**.

$$E: \quad Pd^{II} \rightleftarrows Pd^{III} + e^- \qquad E_1 \tag{1}$$
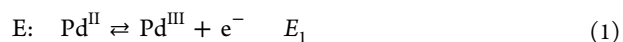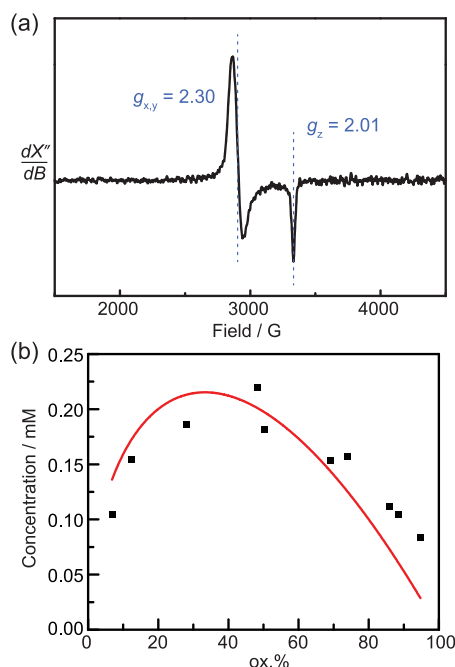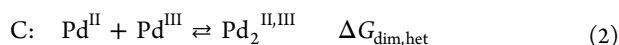
Figure 5. (a) Background-corrected X-band EPR spectrum of **2** at 60 K. (b) (Black squares) EPR-measured spin concentrations versus ox. %. Total Pd concentration was 9.3 mM. $Cu^{II}SO_4$ dissolved in the same medium was used as a spin quantification standard (see the Supporting Information, section 7 for details). (Red line) Calculated $[Pd_2^{II,III}]$ from a least-squares fitting of eq 7 to the EPR-measured spin concentrations.

$$C: \quad Pd^{II} + Pd^{III} \rightleftharpoons Pd_2^{II,III} \qquad \Delta G_{dim,het} \qquad (2)$$

$$E: \quad Pd_2^{II,III} \rightleftharpoons Pd^{III}_2 + e^- \qquad E_2 \qquad (3)$$

In order to determine which radical intermediate, Pd^{III} or $Pd_2^{II,III}$, gives rise to the observed EPR signal, we prepared a series of solutions containing the same total Pd ion concentration but with varying ratios of Pd^{II} and Pd^{III}_2 and measured the spin concentrations (see section 7 in the Supporting Information for details of sample preparation and data collection). The measured spin concentrations are plotted vs ox.% $\equiv \frac{2[Pd^{III}_2]}{[Pd^{III}] + 2[Pd^{III}_2]}$ in Figure 5b. Since Pd^{III} arises from fragmentation of Pd^{III}_2 (eq 4), its concentration is expected to increase monotonically with ox.% (eq 5). In contrast, the $[Pd_2^{II,III}]$ should display a maximum at intermediate levels of oxidation because it arises from the comproportionation of Pd^{II} and Pd^{III}_2 (eqs 6 and 7). Thus, the observed parabolic trend (Figure 5b, black squares) supports assignment of this signal to the mixed-valent dimer, $Pd_2^{II,III}$, rather than the monomeric Pd^{III} intermediate. The maximum $[Pd_2^{II,III}]$ at equilibrium was <5% of the total Pd concentration across all ox.%.

$$2Pd^{III} \rightleftharpoons Pd^{III}_2 \qquad \Delta G_{dim,hom} \qquad (4)$$
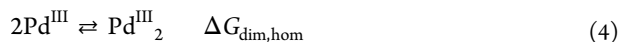
$$[Pd^{III}] = \sqrt{\frac{[Pd^{III}_2]}{K_{dim,hom}}} = \sqrt{\frac{[Pd]_{total}(ox.\%)}{2K_{dim,hom}}} \qquad (5)$$

$$2Pd^{II} + Pd^{III}_2 \rightleftharpoons 2Pd_2^{II,III} \qquad \Delta G_{comp} \qquad (6)$$

$$[Pd_2^{II,III}] = \sqrt{K_{comp}[Pd^{II}]^2[Pd^{III}_2]}$$
$$= \sqrt{\frac{K_{comp}[Pd]_{total}^3}{2}(1 - ox.\%)^2(ox.\%)} \qquad (7)$$

The equilibrium concentration data in Figure 5b yield the thermodynamic stability of this mixed-valent intermediate relative to Pd^{II} and Pd^{III}_2. Fitting eq 7 to the data (Figure 5b, red line), we obtained $K_{comp} = 0.78 \pm 0.11$ M^{-1} and $\Delta G_{comp} = 0.15 \pm 0.08$ kcal mol^{-1}. While the standard comproportionation free energy is slightly positive, due to the low total Pd concentration of our solutions (<10 mM), the $Pd_2^{II,III}$ in our samples is driven toward disproportionation to $2Pd^{II} + Pd^{III}_2$. Together, this analysis establishes that the EPR signal in **2** arises from a $Pd_2^{II,III}$ species formed from minor-equilibrium comproportionation of Pd^{III}_2 and residual Pd^{II}.

Structure of $Pd_2^{II,III}$. To be consistent with the structural model for Pd^{III}_2 put forward in the previous section, the $Pd_2^{II,III}$ complex is expected to have an incipient Pd–Pd bond with a bond order of 0.5. The unpaired electron would reside in the M–M σ^* orbital formed from the overlap of the d_{z2} orbitals along the Pd–Pd bond axis.[9,55] Indeed, the axial EPR signal with $g_{x,y} > g_z$ is consistent with the d_{z2} character of the SOMO[54] and with the spectra of other mixed-valent $Pd_2^{II,III}$ complexes in the literature.[12,52,55] Furthermore, the g-tensor anisotropy of our dimer is exceptionally high, $g_{x,y} = 2.30$ and $g_z = 2.01$; the spread in g components is the greatest among those of reported $Pd_2^{II,III}$ complexes.[12,52,55] This anisotropy indicates low metal–ligand covalency, as would be expected for the hard $H_xSO_4^{(x-2)}$ ligands.[56]

Electrochemical data are also consistent with a formally mixed-valent dimer with a half-order Pd–Pd bond. Prior voltammetric data recorded on FTO electrodes (Figure S2) was insufficient for quantitative determination of E_1 and E_2 due the convolution of slow ET kinetics and an unknown rate constant for the chemical step in the *ECE* mechanism. Using a combination of a Pt electrode with faster ET kinetics and low Pd^{II} concentrations to slow the dimerization C step, we were able to observe a chemically reversible $Pd^{II/III}$ oxidation wave at a midpoint potential of 1.69 V vs SSE (saturated Ag_2SO_4/Ag) (Figure S13). Because the voltammetric features indicated adsorption of Pd^{III} on the Pt electrode surface, this is a lower limit for the value of E_1 (see the Supporting Information, section 8 for details). As for E_2, it is equal to the standard redox potential for the overall Pd^{II}/Pd^{III}_2 redox process minus $\Delta G_{comp}/(2F)$ (see the Supporting Information, section 8 for derivation); therefore, we used open circuit measurements of mixed solutions of Pd^{II} and Pd^{III}_2 (Figure S15) to extract $E_2 = 1.49$ V. This analysis establishes that $Pd_2^{II,III}$ is easier to oxidize by >200 mV than Pd^{II} and is consistent with a M–M σ^* SOMO in $Pd_2^{II,III}$ that is significantly higher in energy than the native d_{z2} orbital in square-planar Pd^{II}. Together, the EPR and electrochemical data support the intermediacy of an $S = \frac{1}{2}$ $Pd_2^{II,III}$ complex, containing a half-order Pd–Pd bond, formed en route to Pd^{III}_2.

Structural and Thermochemical Basis for Electrochemical Pd^{III}_2 Formation. The foregoing structural and spectroscopic insights provide a basis for understanding the unusual *ECE* mechanism that forms Pd^{III}_2 by electrochemical oxidation of Pd^{II}.

Driving Force for Dimerization. The viability of the *ECE* mechanism and the formation of Pd^{III}_2 require thermodynamically accessible dimerization reactions (eqs 2 and 4). The

aforementioned ΔG_{comp}, E_1, and E_2 values allow us to compute free energies of dimerization for both $Pd_2^{II,III}$ and Pd^{III}_2. In Scheme 1, we summarize the set of equilibria describing the Pd

Scheme 1. Summary of the Reactions between Pd^{II}, Pd^{III}_2, Pd^{III}, and $Pd_2^{II,III}$
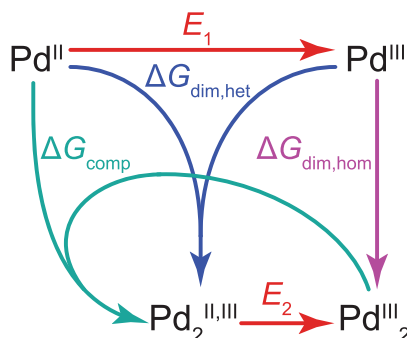
system: E_1, $\Delta G_{dim,het}$, and E_2 are as defined in eqs 1−3, and $\Delta G_{dim,hom}$ and ΔG_{comp} are in eqs 4 and 6. Hess's law provides

$$\Delta G_{dim,het} = \Delta G_{comp} + F(E_2 - E_1) \tag{8}$$

$$\Delta G_{dim,hom} = \Delta G_{comp} + 2F(E_2 - E_1) \tag{9}$$

(see the Supporting Information, section 8 for derivations). From $\Delta G_{comp} = 0.15$ kcal mol^{-1} and $E_2 - E_1 < -0.2$ V, we compute that $Pd_2^{II,III}$ and Pd^{III}_2 are stabilized relative to their constituent monomers by more than 4.5 and 9.1 kcal/mol, respectively. Despite homodimerization being more thermo-dynamically favored relative to heterodimerization, electro-chemical kinetic data establish that heterodimerization is kinetically dominant under voltammetric conditions leading to an *ECE* sequence in which the *C* step is the spontaneous heterodimerization reaction. This analysis highlights the high preference for dimerization of the Pd centers in this system that serves to promote *ECE* oxidation and Pd^{III}_2 formation.

M−M and M−L Bonding Drive ECE Formation of Pd^{III}_2. The *ECE* sequence for the oxidation of Pd^{II} to Pd^{III}_2 involves not only M−M bond formation but also the binding of two axial $H_xSO_4^{(x-2)}$ ligands, both of which contribute to the dimerization free energies for $Pd^{II} + Pd^{III}$ and $Pd^{III} + Pd^{III}$. According to eqs 8 and 9, for any given ΔG_{comp}, both $\Delta G_{dim,het}$ and $\Delta G_{dim,hom}$ become more favorable with a larger degree of potential inversion, $|E_2 - E_1|$. Thus, the 200 mV potential inversion that we observed corresponds to an increased favorability of dimerization and contains contributions from M−M and two axial M−L bonds. Since the sulfuric acid medium contains an abundance of ligating ions, we cannot directly measure the contribution of M−L bonding relative to that of M−M bonding. However, it is noteworthy that electrochemical oxidation of ligand-bridged Pd^{II}_2 precursors in noncoordinating electrolyte media typically proceeds via sequential oxidation without potential inversion,[4,12,57,58] while the addition of 2 equiv of Cl$^-$ transforms two sequential 1-e$^-$ waves in the CV to a single 2-e$^-$ wave, indicating potential inversion and facile oxidation to Pd^{III}_2.[59,60] Likewise, Pd^{II} to Pd^{III}_2 oxidation is facile with chemical oxidants (e.g., PhICl$_2$, PhI(OAc)$_2$) which simultaneously transfer holes *and* ligands to the Pd centers. These observations suggest that, in addition to M−M bonding, axial ligation is also a critical factor for driving potential inversion, Pd dimerization, and facile oxidation.

The combined roles of M−M and M−L bonding in causing dimerization and potential inversion can be rationalized using the qualitative Walsh diagram in Scheme 2 that illustrates the

Scheme 2. Qualitative Walsh Diagram Depicting Changes in Orbital Energies upon Pd−Pd and Pd−L (L: Axial Ligand) Bond Formation
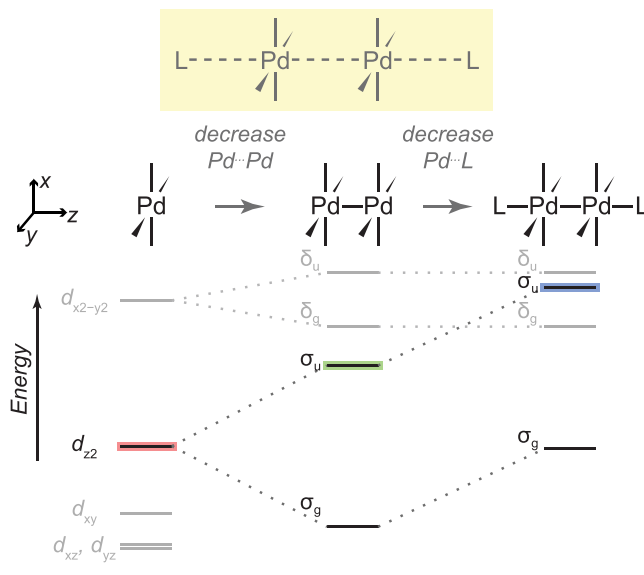
change in the energies of Pd d$_{z^2}$ orbitals with decreased M−M and M−L (L: axial ligand) distances. Absent significant change in structure, electrostatic considerations dictate that each successive redox event of a given compound is more difficult than the previous, i.e., redox potentials become more positive for sequential oxidations. Thus, a potential inversion requires that bonding-induced changes in orbital energetics substan-tially overcome this electrostatic effect. Ligand-bridged Pd^{II}_2 complexes in the literature, whose electrochemistry does not exhibit potential inversion, display some M−M bonding character prior to oxidation.[61] Thus when these complexes are oxidized in noncoordinating media, both electrons are sourced from the M−M σ* orbital (Scheme 2, green) and $E_1 < E_2$. Only the slight contraction of the M−M distance upon the first oxidation, which raises the M−M σ*, contributes to attenuating the non-inverted potential separation between E_1 and E_2. In contrast, in our system, the first electron is removed from the d$_{z^2}$ orbital of monomeric square-planar Pd^{II} (Scheme 2, red) and the second electron is sourced from a putative $Pd_2^{II,III}$ intermediate that is coordinatively saturated (Scheme 2, blue). As illustrated in the scheme, the axial ligands, L, drive up the M−M σ* orbital and contribute to the inversion between E_1 and E_2. Indeed, MOs of one of the calculated Pd^{III}_2 structures in Figure 4 show that the M−M σ* orbital rises in energy so dramatically that it resides above the M−M δ orbital (Figure S19). Since the M−M δ orbital would be much higher than the d$_{z^2}$ orbital of monomeric Pd, this final orbital arrangement is in line with the inversion of E_1 and E_2. In sum, the combined effect of axial ligand binding and M−M bond formation that occurs as part of the *C* step in the *ECE* mechanism drives up the energy of the d$_{z^2}$ orbital, leads to potential inversion, and enables the Pd^{III} dimer formation. This analysis highlights the important role of the sulfuric acid media in facilitating rapid ligand binding toward electrochemical

generation of a potent Pd^{III} dimer for methane C−H functionalization

CONCLUSIONS

Using a combination of spectroscopic techniques, we have assembled structural models of the key high-valent Pd$_2$ intermediates involved in rapid electrochemical methane functionalization and quantified the thermodynamics of spontaneous dimerization. X-ray absorption and Raman spectroscopies indicate that the product of electrochemical Pd^{II} oxidation is a Pd^{III} dimer with a Pd−Pd bond and a 5-fold O atom coordination by H$_x$SO$_4^{(x−2)}$ at each Pd center. EPR spectroscopy establishes the presence of a minor-equilibrium mixed-valent Pd$_2^{II,III}$ intermediate in the *ECE* mechanism for Pd^{II} oxidation. The measured comproportionation free energies and redox potentials for key species in the oxidation sequence enabled quantification of negative free energies for Pd dimerization. The favorable dimerization free energy and large potential inversion arise from the combined effect of M−M and axial M−L bonding interactions that form during the *C* step of the *ECE* oxidation sequence. Together, these studies establish the core structure of Pd$^{III}_2$ as well as a structural basis for its unusual *ECE* formation mechanism, thereby enabling the design of new electrocatalytic oxidation sequences mediated by high-valent Pd complexes.

ASSOCIATED CONTENT

Ⓢ Supporting Information

The Supporting Information is available free of charge at https://pubs.acs.org/doi/10.1021/jacs.0c05894.

> Details of sample preparation, spectroscopic measurements, concentration determination of the Pd species, electrochemical measurements, derivation of equations, and DFT computation (PDF)
>
> Structure files in .xyz format (ZIP)

AUTHOR INFORMATION

Corresponding Authors

Christopher H. Hendon − *Department of Chemistry and Biochemistry, University of Oregon, Eugene, Oregon 97403, United States;* Ⓞ orcid.org/0000-0002-7132-768X; Email: chendon@uoregon.edu

Jeffrey T. Miller − *Davidson School of Chemical Engineering, Purdue University, West Lafayette, Indiana 47907, United States;* Ⓞ orcid.org/0000-0002-6269-0620; Email: jeffrey-t-miller@purdue.edu

Yogesh Surendranath − *Department of Chemistry, Massachusetts Institute of Technology, Cambridge, Massachusetts 02139, United States;* Ⓞ orcid.org/0000-0003-1016-3420; Email: yogi@mit.edu

Authors

R. Soyoung Kim − *Department of Chemistry, Massachusetts Institute of Technology, Cambridge, Massachusetts 02139, United States;* Ⓞ orcid.org/0000-0001-7912-7351

Evan C. Wegener − *Davidson School of Chemical Engineering, Purdue University, West Lafayette, Indiana 47907, United States*

Min Chieh Yang − *Department of Chemistry and Biochemistry, University of Oregon, Eugene, Oregon 97403, United States*

Matthew E. O'Reilly − *Department of Chemistry, Massachusetts Institute of Technology, Cambridge, Massachusetts 02139, United States*

Seokjoon Oh − *Department of Chemistry, Massachusetts Institute of Technology, Cambridge, Massachusetts 02139, United States;* Ⓞ orcid.org/0000-0002-8980-5213

Complete contact information is available at:
https://pubs.acs.org/10.1021/jacs.0c05894

Notes

The authors declare no competing financial interest.

ACKNOWLEDGMENTS

REFERENCES

(1) Powers, I. G.; Uyeda, C. Metal-Metal Bonds in Catalysis. *ACS Catal.* **2017**, *7* (2), 936−958.

(2) Kornecki, K. P.; Berry, J. F.; Powers, D. C.; Ritter, T. Metal-Metal Bond-Containing Complexes as Catalysts for C-H Functionalization. In *Progress in Inorganic Chemistry*; Karlin, K. D., Ed.; John Wiley & Sons, Inc.: Hoboken, NJ, U.S., 2014; Vol. 58, pp 225−302.

(3) Berry, J. F.; Lu, C. C. Metal-Metal Bonds: From Fundamentals to Applications. *Inorg. Chem.* **2017**, *56* (14), 7577−7581.

(4) Powers, D. C.; Geibel, M. A. L.; Klein, J. E. M. N.; Ritter, T. Bimetallic Palladium Catalysis: Direct Observation of Pd(III)-Pd(III) Intermediates. *J. Am. Chem. Soc.* **2009**, *131* (47), 17050−17051.

(5) Hickman, A. J.; Sanford, M. S. High-Valent Organometallic Copper and Palladium in Catalysis. *Nature* **2012**, *484* (7393), 177−185.

(6) Vedernikov, A. N. PdII/PdIV Redox Couple Mediated C−X Bond Formation. In *C−H and C−X Bond Functionalization: Transition Metal Mediation*; Ribas, X., Ed.; The Royal Society of Chemistry: Cambridge, U.K., 2013; pp 108−121; Chapter 4.

(7) Khusnutdinova, J. R.; Mirica, L. M. Organometallic Pd^{III} Complexes in C−C and C−Heteroatom Bond Formation Reactions. In *C−H and C−X Bond Functionalization: Transition Metal Mediation*; Ribas, X., Ed.; The Royal Society of Chemistry: Cambridge, U.K., 2013; Chapter 5, pp 122−158.

(8) Powers, D. C.; Lee, E.; Ariafard, A.; Sanford, M. S.; Yates, B. F.; Canty, A. J.; Ritter, T. Connecting Binuclear Pd(III) and Mononuclear Pd(IV) Chemistry by Pd-Pd Bond Cleavage. *J. Am. Chem. Soc.* **2012**, *134* (29), 12002−12009.

(9) Powers, D. C.; Ritter, T. Bimetallic Redox Synergy in Oxidative Palladium Catalysis. *Acc. Chem. Res.* **2012**, *45* (6), 840−850.

(10) Powers, D. C.; Ritter, T. A Transition State Analogue for the Oxidation of Binuclear Palladium(II) to Binuclear Palladium(III) Complexes. *Organometallics* **2013**, *32* (7), 2042−2045.

(11) Chuang, G. J.; Wang, W.; Lee, E.; Ritter, T. A Dinuclear Palladium Catalyst for α-Hydroxylation of Carbonyls with O₂. *J. Am. Chem. Soc.* **2011**, *133* (6), 1760−1762.

(12) Dudkina, Y. B.; Kholin, K. V.; Gryaznova, T. V.; Islamov, D. R.; Kataeva, O. N.; Rizvanov, I. K.; Levitskaya, A. I.; Fominykh, O. D.; Balakina, M. Y.; Sinyashin, O. G.; Budnikova, Y. H. Redox Trends in Cyclometalated Palladium(II) Complexes. *Dalt. Trans.* **2017**, *46* (1), 165−177.

(13) Budnikova, Y.; Dudkina, Y.; Khrizanforov, M. Redox-Induced Aromatic C−H Bond Functionalization in Metal Complex Catalysis from the Electrochemical Point of View. *Inorganics* **2017**, *5* (4), 70.

(14) Estevan, F.; Hirva, P.; Sanaú, M.; Úbeda, M. Stability of Dinuclear Phosphane Palladium(III) Complexes: A DFT Approach. *Organometallics* **2018**, *37* (18), 2980−2990.

(15) Zhang, L. L.; Zhang, L.; Li, S. J.; Fang, D. C. DFT Studies on the Distinct Mechanisms of C-H Activation and Oxidation Reactions Mediated by Mononuclear- and Binuclear-Palladium. *Dalt. Trans.* **2018**, *47* (17), 6102−6111.

(16) Wenzel, M. N.; Owens, P. K.; Bray, J. T. W.; Lynam, J. M.; Aguiar, P. M.; Reed, C.; Lee, J. D.; Hamilton, J. F.; Whitwood, A. C.; Fairlamb, I. J. S. Redox Couple Involving NO_x in Aerobic Pd-Catalyzed Oxidation of sp^3-C−H Bonds: Direct Evidence for Pd−NO_3^-/NO_2^- Interactions Involved in Oxidation and Reductive Elimination. *J. Am. Chem. Soc.* **2017**, *139* (3), 1177−1190.

(17) Haines, B. E.; Xu, H.; Verma, P.; Wang, X. C.; Yu, J. Q.; Musaev, D. G. Mechanistic Details of Pd(II)-Catalyzed C-H Iodination with Molecular I₂: Oxidative Addition vs Electrophilic Cleavage. *J. Am. Chem. Soc.* **2015**, *137* (28), 9022−9031.

(18) Ariafard, A.; Hyland, C. J. T.; Canty, A. J.; Sharma, M.; Brookes, N. J.; Yates, B. F. Ligand Effects in Bimetallic High Oxidation State Palladium Systems. *Inorg. Chem.* **2010**, *49* (23), 11249−11253.

(19) Kärkäs, M. D. Electrochemical Strategies for C−H Functionalization and C−N Bond Formation. *Chem. Soc. Rev.* **2018**, *47* (15), 5786−5865.

(20) Ma, C.; Fang, P.; Mei, T. S. Recent Advances in C-H Functionalization Using Electrochemical Transition Metal Catalysis. *ACS Catal.* **2018**, *8* (8), 7179−7189.

(21) O'Reilly, M. E.; Kim, R. S.; Oh, S.; Surendranath, Y. Catalytic Methane Monofunctionalization by an Electrogenerated High-Valent Pd Intermediate. *ACS Cent. Sci.* **2017**, *3* (11), 1174−1179.

(22) Zimmermann, T.; Soorholtz, M.; Bilke, M.; Schüth, F. Selective Methane Oxidation Catalyzed by Platinum Salts in Oleum at Turnover Frequencies of Large-Scale Industrial Processes. *J. Am. Chem. Soc.* **2016**, *138* (38), 12395−12400.

(23) Mirica, L. M.; Khusnutdinova, J. R. Structure and Electronic Properties of Pd(III) Complexes. *Coord. Chem. Rev.* **2013**, *257* (2), 299−314.

(24) Lu, E.; Liddle, S. T. Group 10 Metal-Metal Bonds. In *Molecular Metal-Metal Bonds*; Wiley-VCH Verlag GmbH & Co. KGaA:: Weinheim, Germany, 2015; pp 325−395.

(25) Khusnutdinova, J. R.; Rath, N. P.; Mirica, L. M. Dinuclear Palladium(III) Complexes with a Single Unsupported Bridging Halide Ligand: Reversible Formation from Mononuclear Palladium(II) or Palladium(IV) Precursors. *Angew. Chem., Int. Ed.* **2011**, *50* (24), 5532−5536.

(26) Eitel, S. H.; Bauer, M.; Schweinfurth, D.; Deibel, N.; Sarkar, B.; Kelm, H.; Krüger, H. J.; Frey, W.; Peters, R. Paramagnetic Palladacycles with Pd^III Centers Are Highly Active Catalysts for Asymmetric Aza-Claisen Rearrangements. *J. Am. Chem. Soc.* **2012**, *134* (10), 4683−4693.

(27) Zhang, B.; Yan, X.; Guo, S. Synthesis of Well-Defined High-Valent Palladium Complexes by Oxidation of Their Palladium(II) Precursors. *Chem. - Eur. J.* **2020**, *26* (43), 9430−9444.

(28) Gruzensky, P. M. Crystallization of Anhydrous Copper Sulfate from Sulfuric Acid - Ammonium Sulfate Mixtures. *J. Res. Natl. Bur. Stand., Sect. A* **1964**, *68A* (3), 313.

(29) Dahmen, T.; Rittner, P.; Böger-Seidl, S.; Gruehn, R. Beiträge Zum Thermischen Verhalten von $PdSO_4 \cdot 2H_2O$ Und $PdSO_4 \cdot 0,75H_2O$ Sowie Zur Struktur von M-$PdSO_4$. *J. Alloys Compd.* **1994**, *216* (1), 11−19.

(30) Kornecki, K. P.; Briones, J. F.; Boyarskikh, V.; Fullilove, F.; Autschbach, J.; Schrote, K. E.; Lancaster, K. M.; Davies, H. M. L.; Berry, J. F. Direct Spectroscopic Characterization of a Transitory Dirhodium Donor-Acceptor Carbene Complex. *Science (Washington, DC, U. S.)* **2013**, *342* (6156), 351−354.

(31) Colpas, G. J.; Maroney, M. J.; Bagyinka, C.; Kumar, M.; Willis, W. S.; Suib, S. L.; Mascharak, P. K.; Baidya, N. X-Ray Spectroscopic Studies of Nickel Complexes, with Application to the Structure of Nickel Sites in Hydrogenases. *Inorg. Chem.* **1991**, *30* (5), 920−928.

(32) Cramer, S. P.; Eidsness, M. K.; Pan, W. H.; Morton, T. A.; Ragsdale, S. W.; DerVartanian, D. V.; Ljungdahl, L. G.; Scott, R. A. X-Ray Absorption Spectroscopic Evidence for a Unique Nickel Site in Clostridium Thermoaceticum Carbon Monoxide Dehydrogenase. *Inorg. Chem.* **1987**, *26* (15), 2477−2479.

(33) Getsoian, A.; Das, U.; Camacho-Bunquin, J.; Zhang, G.; Gallagher, J. R.; Hu, B.; Cheah, S.; Schaidle, J. A.; Ruddy, D. A.; Hensley, J. E.; Krause, T. R.; Curtiss, L. A.; Miller, J. T.; Hock, A. S. Organometallic Model Complexes Elucidate the Active Gallium Species in Alkane Dehydrogenation Catalysts Based on Ligand Effects in Ga K-Edge XANES. *Catal. Sci. Technol.* **2016**, *6* (16), 6339−6353.

(34) Zhang, G.; Li, J.; Deng, Y.; Miller, J. T.; Kropf, a J.; Bunel, E. E.; Lei, A. Structure-Kinetic Relationship Study of Organozinc Reagents. *Chem. Commun. (Cambridge, U. K.)* **2014**, *50* (63), 8709−8711.

(35) Campbell, M. G.; Powers, D. C.; Raynaud, J.; Graham, M. J.; Xie, P.; Lee, E.; Ritter, T. Synthesis and Structure of Solution-Stable One-Dimensional Palladium Wires. *Nat. Chem.* **2011**, *3* (12), 949−953.

(36) Blackburn, N. J.; Barr, M. E.; Woodruff, W. H.; van der Ooost, J.; de Vries, S. Metal-Metal Bonding in Biology: EXAFS Evidence for a 2.5 Å Copper-Copper Bond in the CUA Center of Cytochrome Oxidase. *Biochemistry* **1994**, *33* (34), 10401−10407.

(37) Jalilehvand, F.; Maliarik, M.; Mink, J. J.; Sandström, M.; Ilyukhin, A.; Glaser, J. Structure Studies of Dimeric $[Pt_2(CN)_{10}]^{4-}$ Pentacyanoplatinum(III) and Monomeric Pentacyanoplatinum(IV) Complexes by EXAFS, Vibrational Spectroscopy, and X-Ray Crystallography. *J. Phys. Chem. A* **2002**, *106* (14), 3501−3516.

(38) Tanase, T.; Kawahara, K.; Ukaji, H.; Kobayashi, K.; Yamazaki, H.; Yamamoto, Y. Electrochemical Preparation and Characterization of Binuclear Palladium(I) Complexes Containing Aromatic Isocyanide and Chelating Diphosphine Ligands. *Inorg. Chem.* **1993**, *32* (17), 3682−3688.

(39) Fernández, E. J.; Hardacre, C.; Laguna, A.; Lagunas, M. C.; López-de-Luzuriaga, J. M.; Monge, M.; Montiel, M.; Olmos, M. E.; Puelles, R. C.; Sánchez-Forcada, E. Multiple Evidence for Gold(I)-Silver(I) Interactions in Solution. *Chem. - Eur. J.* **2009**, *15* (25), 6222−6233.

(40) Asakura, K.; Kitamura-Bando, K.; Isobe, K.; Arakawa, H.; Iwasawa, Y. Metal-Assisted CO Insertion Reaction on a New Surface Rhodium Dimer Catalyst Observed by an in Situ EXAFS Technique. *J. Am. Chem. Soc.* **1990**, *112* (8), 3242−3244.

(41) Askham, F. R.; Stanley, G. G.; Marques, E. C. A New Type of Transition-Metal Dimer Based on a Hexaphosphine Ligand System: $Co_2(CO)_4(eHTP)^{2+}$ (eHTP = $(Et_2PCH_2CH_2)_2PCH_2P$-$(CH_2CH_2PEt_2)_2$). *J. Am. Chem. Soc.* **1985**, *107* (25), 7423−7431.

(42) Muraveiskaya, G. S.; Orlova, V. S.; Evstaf'eva, O. N. Reaction of $K_2Pt(NO_2)_4$ with H_2SO_4 and the Preparation of Sulphato-Compounds of Platinum. *Russ. J. Inorg. Chem.* **1974**, *19* (4), 1030−1035 (561−566)..

(43) Chen, M.; Wei, C.; Tao, J.; Wu, X.; Huang, N.; Zhang, G.; Li, L. Supramolecular Polymers Self-Assembled from Trans-Bis-(Pyridine) Dichloropalladium(II) and Platinum(II) Complexes. *Chem. - Eur. J.* **2014**, *20* (10), 2812−2818.

(44) Gager, H. M.; Lewis, J.; Ware, M. J. Metal−Metal Stretching Frequencies in Raman Spectra. *Chem. Commun. (London)* **1966**, *0* (17), 616−617.

(45) Miskowski, V. M.; Smith, T. P.; Loehr, T. M.; Gray, H. B. Properties of Metal-Metal Single Bonds. Vibrational and Electronic Spectra of Binuclear Rhodium(II) and Iridium(II) Isocyanide Complexes with Comparisons to Decacarbonyldimanganese [$Mn_2(CO)_{10}$]. *J. Am. Chem. Soc.* **1985**, *107* (26), 7925−7934.

(46) Newman, R. A.; Martin, D. S.; Dallinger, R. F.; Woodruff, W. H.; Stiegman, A. E.; Che, C. M.; Schaefer, W. P.; Miskowski, V. M.; Gray, H. B. Vibrational and Electronic Spectra of Tetrasulfatodiplatinate(2-) Complexes. *Inorg. Chem.* **1991**, *30* (24), 4647−4654.

(47) Orlova, V. S.; Muraveiskaya, G. S.; Evstaf'eva, O. N. Preparation of the Sulphato-Coplexes of Platinum Mn[Pt2(SO4)-4X2].H2O and Mn[Pt2(SO4)4XY].H2O. *Russ. J. Inorg. Chem.* **1975**, *20*, 1340−1346.

(48) Miskowski, V. M.; Dallinger, R. F.; Christoph, G. G.; Morris, D. E.; Spies, G. H.; Woodruff, W. H. Assignment of the Rhodium-Rhodium Stretching Frequency in $Rh_2(O_2CCH_3)_4L_2$ Complexes and the Crystal and Molecular Structure of $[C(NH_2)_3]_2[Rh-(O_2CCH_3)_4Cl_2]$. Relationship between Vibrational Spectra and Structure. *Inorg. Chem.* **1987**, *26* (13), 2127−2132.

(49) Allemand, C. D. Depolarization Ratio Measurements in Raman Spectrometry. *Appl. Spectrosc.* **1970**, *24* (3), 348−353.

(50) Jaworski, J. N.; McCann, S. D.; Guzei, I. A.; Stahl, S. S. Detection of Palladium(I) in Aerobic Oxidation Catalysis. *Angew. Chem., Int. Ed.* **2017**, *56* (13), 3605−3610.

(51) Cook, A. K.; Sanford, M. S. Mechanism of the Palladium-Catalyzed Arene C−H Acetoxylation: A Comparison of Catalysts and Ligand Effects. *J. Am. Chem. Soc.* **2015**, *137* (8), 3109−3118.

(52) Berry, J. F.; Bill, E.; Bothe, E.; Cotton, F. A.; Dalal, N. S.; Ibragimov, S. A.; Kaur, N.; Liu, C. Y.; Murillo, C. A.; Nellutla, S.; North, J. M.; Villagrán, D. A Fractional Bond Order of 1/2 in Pd_2^{5+}-Formamidinate Species; the Value of Very High-Field EPR Spectra. *J. Am. Chem. Soc.* **2007**, *129* (5), 1393−1401.

(53) Wang, C. H.; Gao, W. Y.; Ma, Q.; Powers, D. C. Templating Metastable Pd_2 Carboxylate Aggregates. *Chem. Sci.* **2019**, *10* (6), 1823−1830.

(54) Drago, R. S. *Physical Methods in Inorganic Chemistry*, 2nd ed.; Surfside Scientific Publishers: Gainesville, FL, U.S., 1992.

(55) Yao, C. L.; He, L. P.; Korp, J. D.; Bear, J. L. Dipalladium Complexes with N,N′-Diphenylbenzamidine Bridging and Chelating Ligands. Synthesis and Structural and Electrochemical Studies. *Inorg. Chem.* **1988**, *27* (24), 4389−4395.

(56) McAuley, A.; Whitcombe, T. W. Bis(1,4,7-Triazacyclononane)-Palladium(III): Characterization and Reactions of an Unusually Stable Monomeric Palladium(III) Ion. *Inorg. Chem.* **1988**, *27* (18), 3090−3099.

(57) Dudkina, Y. B.; Mikhaylov, D. Y.; Gryaznova, T. V.; Tufatullin, A. I.; Kataeva, O. N.; Vicic, D. A.; Budnikova, Y. H. Electrochemical Ortho Functionalization of 2-Phenylpyridine with Perfluorocarboxylic Acids Catalyzed by Palladium in Higher Oxidation States. *Organometallics* **2013**, *32* (17), 4785−4792.

(58) Nguyen, B. N.; Adrio, L. A.; Albrecht, T.; White, A. J. P.; Newton, M. A.; Nachtegaal, M.; Figueroa, S. J. A.; Hii, K. K. Electronic Structures of Cyclometalated Palladium Complexes in the Higher Oxidation States. *Dalt. Trans.* **2015**, *44* (37), 16586−16591.

(59) Durrell, A. C.; Jackson, M. N.; Hazari, N.; Gray, H. B. Making Carbon-Chlorine Bonds by Dipalladium Electrocatalysis. *Eur. J. Inorg. Chem.* **2013**, *2013* (7), 1134−1137.

(60) Koshevoy, I. O.; Lahuerta, P.; Sanaú, M.; Ubeda, M. A.; Doménech, A. Dinuclear Palladium(II) Compounds with Bridging Cyclometalated Phosphines. Synthesis, Crystal Structure and Electrochemical Study. *J. Chem. Soc. Dalt. Trans.* **2006**, *46*, 5536−5541.

(61) Bercaw, J. E.; Durrell, A. C.; Gray, H. B.; Green, J. C.; Hazari, N.; Labinger, J. A.; Winkler, J. R. Electronic Structures of Pd^{II} Dimers. *Inorg. Chem.* **2010**, *49* (4), 1801−1810.